ARTICLE

CO₂ Coverage on Pd Catalysts Accelerates Oxygen Removal in Oxy-Combustion Systems

Received 00th January 20xx, Accepted 00th January 20xx

DOI: 10.1039/x0xx00000x

Sungyoon Jung^a, Tengfei Cao^b, Rohan Mishra^b, and Pratim Biswas*a,c

Oxy-combustion systems result in enriched CO_2 in the exhaust gases; however, the utilization of the concentrated CO_2 stream from oxy-combustion is limited by remnant O_2 . CH_4 oxidation using Pd catalysts has been found to have a high O_2 -removal efficiency. Here, the effect of the excess CO_2 in the feed stream on O_2 removal with CH_4 oxidation is investigated by combining experimental and theoretical approaches. Experimental results reveal complete CH_4 oxidation without any side-products, and a monotonic increase in the rate of CO_2 generation with increase in CO_2 concentration in the feed stream. Density-functional theory calculations show that high surface coverage of CO_2 on Pd leads to a reduction in the activation energy for the initial dissociation of CH_4 into CH_3 and H, and also the subsequent oxidation reactions. A CO_2 -rich environment in oxy-combustion systems is therefore beneficial for the reduction of oxygen in the exhaust gas.

Introduction

Oxy-combustion systems using enriched O_2 in the feed stream are effective for producing enriched CO_2 in the exhaust gases from power plants. A concentrated CO_2 stream (>63%) in the exhaust gas can be obtained from oxy-combustion systems and can be further utilized for enhanced oil recovery (EOR), conversion to useful products, 7 or sequestration8. However, its applications are hampered by high remnant O_2 concentrations (~3%) that can cause corrosion inside transport pipes. The United States Department of Energy has set the targeted maximum concentration of O_2 to 100 parts per million volume (ppmv) for EOR. This requires efficient strategies to reduce the O_2 concentration in the exhaust gas stream of oxy-combustion systems.

Catalytic CH₄ oxidation has been designed to remove O_2 from the CO_2 stream. Recent studies have shown their positive progress towards effective O_2 removal.¹¹⁻¹³ Supported catalysts using noble metals (e.g., Pd and Pt) and non-noble metals (e.g., Cu) have shown a high removal efficiency of O_2 (>95%) at relatively low temperatures (<773 K).¹¹⁻¹³ The gas composition in the feed stream has been reported to have a significant consequence on the reactions involving O_2 . Kuhn *et al.*¹² reported that under O_2 -rich or near stoichiometric conditions ($O_2/CH_4 = 2$) in the feed stream, complete CH_4 oxidation was the major reaction. However, under O_2 -poor conditions, CO is also generated via dry reforming of CH_4 . Even though CO_2 is the dominant component in the feed stream, there are

only a handful of reports on the effect of excessive CO₂ on O₂ removal and CH₄ oxidation. A recent study reported a linear correlation between the concentration of CO₂ in the feed stream and the conversion rate of O2 under slightly O2-rich conditions (O₂/CH₄≈2.3).¹⁴ Increased efficiency of O₂ removal via complete CH₄ oxidation was observed with an increase in CO2 concentration in the feed stream. However, the underlying mechanisms for these observations are not clear. According to reported studies, a positive correlation between the concentration of the initial component and the reaction rate could be attributed to two different effects, namely the autocatalytic effect and the surface-coverage effect. 15, 16, 17, 18, 19 Autocatalytic effect, i.e., self-replication, defines a reaction in which the product acts as a catalyst. 15 It has been widely applied in various applications such as methanol synthesis in the presence of water¹⁶ and the reaction of CO with OH radical to form CO2 $(CO+OH^{\bullet}\rightarrow CO_2+H^{\bullet})$ in the presence of supercritical CO_2 .¹⁷ In these reactions, the accelerated reaction rate is enabled by a reduction in the activation energy barriers through the creation of new intermediates from the products. 16, 17 The coverage effect could also result in an accelerated reaction rate; however, the product is not involved in the reaction as a catalyst. Instead of directly participating in the reaction, it covers the surface and decreases the activation energy barrier by modifying the surface electronic structure. 18, 19 Currently, there is no clear evidence on which of these two effects result in the accelerated reaction rate of O2 and CH4 oxidation as observed in the experiments.

In this study, the effect of excess CO_2 in the feed stream on the complete CH_4 oxidation reaction was investigated using a combination of experiments and theoretical calculations. Pd-TiO $_2$ nanoparticle catalysts were synthesized and were used to examine the effect of excess CO_2 in the feed stream on O_2 removal. Four different CO_2 concentrations in the feed stream were studied. Density-functional theory (DFT) calculations were used to understand the mechanisms of excess CO_2 on O_2 removal. Both surface coverage and autocatalytic effects were

^{a.} Department of Energy, Environmental and Chemical Engineering, Washington University in St. Louis, St. Louis, MO 63130, USA

b. Department of Mechanical Engineering and Materials Science, and Institute of Materials Science and Engineering, Washington University in St. Louis, St. Louis, MO 63130, USA

Department of Chemical, Environmental and Materials Engineering, University of Miami, Coral Gables, FL 33146, USA. E-mail: pbiswas@miami.edu
 †Electronic Supplementary Information (ESI) available:
 See DOI: 10.1039/x0xx00000x

examined by changing CO_2 coverage and by analysing their effect on the formation of new intermediates via CO_2 -involved side reactions. Our experiments show CH_4 oxidation as the primary reaction. Further, the generation rate of CO_2 is accelerated with an increase in the CO_2 concentration in the feed stream. DFT calculations on Pd (111) surface show that the surface CO_2 coverage determines the rate-limiting step of the CH_4 oxidation reaction, and increased surface coverage of CO_2 reduces the barriers for CH_4 dissociation.

Materials and methods

Materials preparation, characterization, and experimental procedure are described first, followed by computational details.

Synthesis of catalysts with a flame aerosol reactor (FLAR)

Pd-TiO₂ catalyst was synthesized by using a flame aerosol reactor (FLAR). Detailed information of the synthesis procedure is elucidated elsewhere.14 Briefly, a bubbler was used to introduce titanium tetraisopropoxide (TTIP, 99.7%, Sigma-Aldrich) precursor vapor into FLAR. Appropriate amount of palladium acetylacetonate (Pd(acac)₂, 97%, Sigma-Aldrich) was dissolved in xylene (reagent grade, Sigma-Aldrich) and acetonitrile (99.8%, Sigma-Aldrich) mixture (2:1, v/v) to prepare 1.3 M of the precursor solution. The mixed precursor solution was introduced into FLAR via a Collison nebulizer with N2 carrier gas. Both precursors (TTIP and palladium acetylacetonate) were introduced into FLAR through the center port of the reactor. CH₄ and O₂ were introduced into FLAR through the second and the third ports of the reactor with flow rates of 0.35 L min⁻¹ and 2.5 L min⁻² ¹, respectively. A flame was created via an ignition. Pd-doped TiO₂ nanoparticles were then created in the flame.²⁰ The produced nanoparticles were collected at the end of the system on an isopore membrane filter. The weight percent of Pd on TiO₂ catalyst was confirmed as ~0.76 wt% by inductively coupled plasma mass spectrometry (ICP-MS, Elan DRC ii, PerkinElmer).

The structural properties of the synthesized catalyst were determined using different analytical tools. The morphology and size of the synthesized Pd-TiO $_2$ catalyst was evaluated by scanning transmission electron microscopy (STEM) (JEOL 2100F). The oxidation state of Pd on TiO $_2$ surface was determined by X-ray photoelectron spectroscopy (XPS, Versa probe ii, Physical Electronics). XPS analysis was performed in triplicate and many spots were investigated for STEM analysis to generate representative data.

Detailed experimental setup and procedure for the catalysis experiments are provided elsewhere. He Briefly, 10 mg of the synthesized catalyst was put into a fixed bed reactor. The experiments were performed under a stoichiometric gas composition ($O_2/CH_4=2$), and the concentration of CO_2 in the feed stream was varied from 0 mol m-3 (0%) – 38.6 mol m-3 (95.5%). The concentration of CH_4 in the feed stream was fixed at ~1.5%. Helium gas was used as the balance of the gas, if needed. By controlling the concentration of CO_2 in the feed stream, the effect of excessive amount of CO_2 on O_2 removal was investigated. Atmospheric pressure and temperatures ranging from room temperature to 773 K were applied. A total flow rate of ~3 ml min-1 was controlled by using a mass-flow

controller. The initial, intermediate, and final gas compositions during the O_2 removal via CH_4 oxidation reaction were measured by gas chromatography (GC, 7890B, Agilent Technologies, Inc.) equipped with a porous layer open tubular (PLOT) capillary column and a thermal conductivity detector (TCD). Helium was used as a carrier gas.

Computational details

DFT calculations were performed using the Vienna Ab initio Simulation Package (VASP).²¹ The energy cut-off for the plane waves was set to 450 eV. $1 imes 10^{-6}$ eV was the threshold of energy convergence of the self-consistent loops. During the structure optimization, the convergence criteria for forces on ions was 0.01 eV Å-1. We used projector augmented-wave (PAW) potentials²² and the generalized gradient approximation (GGA) within the Perdew-Burke-Ernzerhof (PBE)²³ parameterization to describe the electron-ion and the electronic exchange-correlation interactions, respectively. The Brillouin zone was sampled with 3×3×1 k-points mesh using the Monkhorst-Pack scheme.²⁴ DFT-D3 method with Becke-Jonson damping²⁵ was used to include Van der Waals interactions between adsorbates and the slab surface. Previous studies^{14, 26, 27} have shown that metallic Pd and/or reduced Pd oxides play a major role in the removal of O2 via CH4 oxidation reaction. Therefore, metallic Pd was used in our calculations. For a face-centered cubic (fcc) metal, its (111) surface has the lowest energy, followed by (100) and (110) surfaces, 28 which implies that (111) facets could be major surfaces of the nanoparticles. Therefore, Pd (111) was used in this study. A slab of (3×3) Pd (111) surface with three layers thickness and 15 Å of vacuum, as shown in Fig S1[†], was created. The atoms in the bottom layer of the slab were fixed to their bulk coordinates and other layers were fully optimized. The adsorption and reactions were carried out on the created Pd (111) surface. Number (n) of adsorbate molecules on the surface corresponds to a coverage of n/9 ML (monolayer). For example, one adsorbate molecule on the surface indicates a coverage of 0.11 (1/9) ML.

The adsorption energy E_{ads} (eV) of molecules is defined as:

$$E_{ads} = E_{adsorbate/slab} - (E_{adsorbate} + E_{slab}),$$
 (1)

where $E_{adsorbate/slab}$, $E_{adsorbate}$, and E_{slab} represent the energy of the adsorbed system, the molecule in the gas phase, and the slab, respectively. A negative adsorption energy indicates that the adsorption of molecules is an exothermic reaction, while a positive adsorption energy indicates an endothermic reaction. Four different high symmetric adsorption sites: top sites (top), bridging ones (bridge) and the hollow sites (fcc, and hcp), as shown in Fig S1 † , were selected to calculate the most favorable adsorption site. The optimized structures of adsorbed molecules are shown in Fig S2 † .

To investigate the transition states and the activation energies (E_a , eV), the nudged elastic-band method (NEB)²⁹ was used to identify the saddle points. 15 or 18 images between initial and final structures were created and used for NEB calculations. The highest energies and the resulting images were assigned activation energies and transition state structures. Zero-point energy (ZPE) corrections³⁰ have been calculated for select cases to determine their effect on the activation energy of CH₄ dissociation reaction.

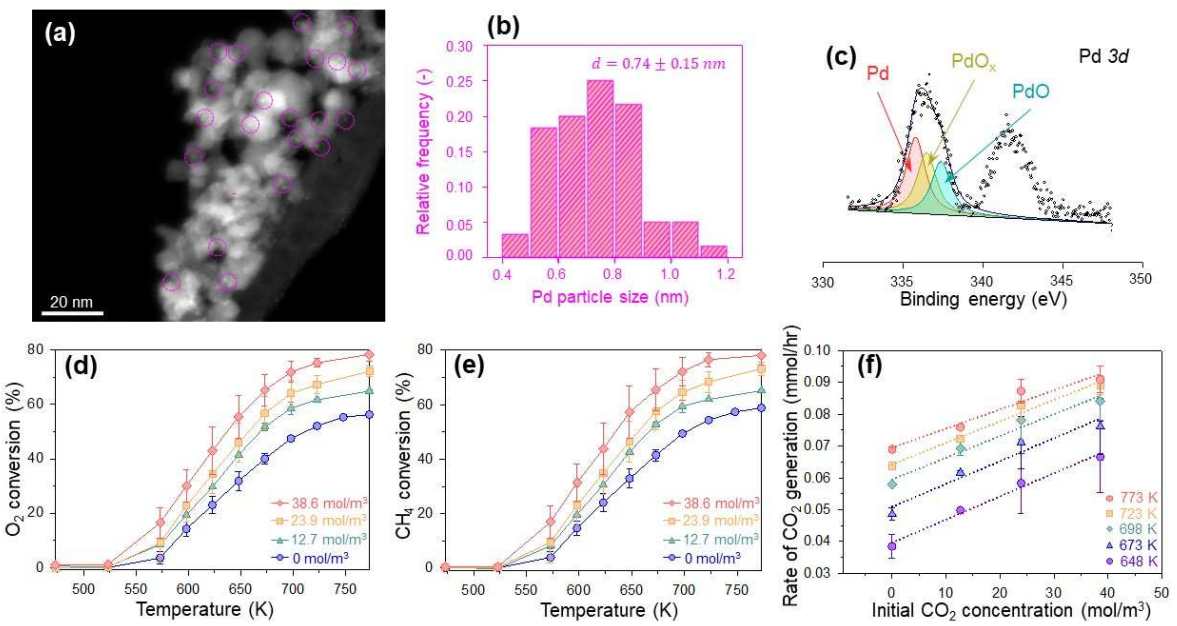


Fig 1. (a) STEM Z-contrast image of Pd-doped TiO_2 nanoparticles. (b) A histogram of the size distributes of Pd clusters. (c) XPS spectra of Pd, conversion of (d) O_2 and (e) CH_4 with increasing temperature and increasing concentration of CO_2 in the feed stream, and (f) the generation rate of CO_2 as a function of initial CO_2 concentration.

Results and discussion

Experimental results

Structure and composition of the Pd-TiO₂ catalysts

The morphology and the size of the synthesized Pd-TiO₂ nanoparticles were investigated by STEM using Z-contrast imaging. A representative image of the nanoparticles is shown in Fig 1a. In this imaging mode, heavier atoms with higher atomic number (Z), such as Pd, appear brighter.³¹ The synthesized TiO₂ nanoparticles were observed to have a spherical shape ($^{\sim}$ 8 nm). Pd clusters were found to be well-dispersed on the TiO₂ supports (bright dots inside pink circles in Fig 1a). The size distribution of Pd clusters was evaluated and is shown in Fig 1b. The average size of Pd clusters was determined to be 0.74 nm \pm 0.15 nm.

The oxidation state of Pd was evaluated using XPS, and the corresponding spectra are shown in Fig 1c. We found that Pd existed as three different species, which were metallic Pd (335.7 eV), intermediate PdO_x (0<x<1) (336.42 eV), and PdO (337.4 eV). 32 According to our recent study, 14 metallic Pd among three Pd species showed a linear dependence to the apparent reaction rate constant, which indicates that metallic Pd plays a major role for O₂ removal. The total surface area of metallic Pd was calculated as $^{\sim}220~\text{cm}^2$ in this study. Previous studies also show that metallic Pd plays a dominant role in O₂ removal and complete CH₄ oxidation. $^{14, 26, 27}$ Therefore, metallic Pd was used for further DFT calculations.

Effect of CO₂ concentration in the feed stream on O₂ removal

To investigate the effect of CO_2 in the feed stream on the O_2 removal via complete CH_4 oxidation, experiments were performed with initial CO_2 concentrations varying from 0 mol m⁻³ to 38.6 mol m⁻³, and with helium as the balance of the gas, under stoichiometric conditions $(O_2/CH_4=2)$. As can be seen in Figs 1d and 1e, both conversion rate of O_2 and CH_4 increased,

when the CO₂ concentration in the feed stream was increased. To clearly see the correlation between the reaction rate and the initial CO₂ concentration, the generation rate of CO₂ versus the initial CO₂ concentration is plotted in Fig 1f. The plot shows that the generation rate of CO₂ is proportional to the initial CO₂ concentration. The generation rate of CO₂ (mmol hr⁻¹) versus the initial concentration of CO₂ (mol m⁻³) at different temperatures can be explained by a linear dependence (R^2 > 0.92). As explained in the introduction part, it can be defined as either an autocatalytic effect or a coverage effect of CO₂. The accelerated reaction rate could be supported by the lower activation energy barriers via creation of new intermediates (autocatalytic effect) or via modification of the surface (surface coverage effect). 16-19 Based on the experimental results, it could be concluded that CO₂ is directly or indirectly involved in the O₂ removal via the complete CH₄ oxidation reaction. To distinguish between the autocatalytic and surface coverage effects, DFT calculations were carried out, and the corresponding results are described in the following sections. It should be noted that, we do not find the generation of H₂ or CO during the reaction, which implies that there is only one reaction, i.e., complete CH₄ oxidation. We also detect the closed values between the reaction rates of CH₄ and half of the reaction rate of O₂ (Table S1), which proves the complete CH₄ reaction. Thereby, the complete CH₄ oxidation reaction was applied for further DFT calculations.

Computational results

CO₂ adsorption on Pd (111)

It has been demonstrated that the CO_2 molecule is first physisorbed and is then chemisorbed on the metal surface.²⁸ In this study, various configurations of CO_2 were considered and their adsorption on Pd was investigated. As depicted in Fig 2, regardless of its initial configuration, CO_2 molecules preferred to be weakly physisorbed on Pd (111) surface. The bond length

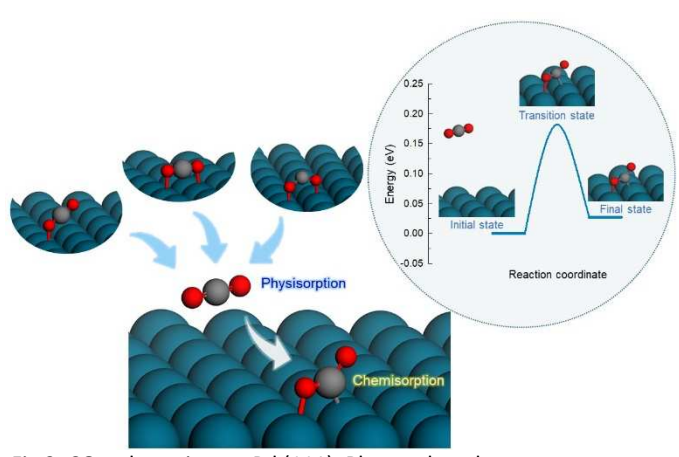


Fig 2. CO_2 adsorption on Pd (111). Blue, red, and grey atoms represent Pd, O, and C, respectively. Three models in the inset show the initial structures of CO_2 .

between C and O atoms was $^{\sim}1.18$ Å and the angle of O-C-O was 179.3°. The distance between O atom and topmost Pd (111) surface was 3.15 Å. The physisorbed CO₂ molecule could then transform into chemisorption by forming O-Pd bonds and exist in a bidentate configuration. The lengths between C and O atoms were $^{\sim}1.21$ Å and $^{\sim}1.26$ Å, and the angle of O-C-O was 138°. The distance between O atom and topmost Pd was 2.16

Å. The adsorption energy of the chemisorbed CO₂ on Pd (111) was calculated to be 0.03 eV, which is similar to the previously reported value on Pd (111).33 It is much lower than the reported adsorption values on non-metal surfaces such as Si- and Sedoped graphene (0.18 eV and 0.21 eV).30 It indicates that the noble metal creates a favorable environment for CO₂ adsorption on its surface, while CO₂ desorption can also easily occur with its lower CO₂ capture ability. The activation energy between the gaseous CO2 and the chemisorbed CO2 was calculated as ~0.18 eV (Fig 2). This small activation energy barrier indicates that CO₂ could chemisorb on Pd (111) surface in the reaction. However, the final state of the chemisorbed CO₂ is slightly uphill, which implies that the reaction is a slightly endothermic reaction. Therefore, chemisorbed CO₂ molecules could easily desorb from Pd (111) surface. However, under our experimental condition, i.e., with excessive CO₂ concentration in the initial gas stream, some CO2 molecules could stay on Pd (111) surface even though other CO₂ molecules might desorb it. In the next section, the influence of CO2 coverage on Pd (111) was examined.

CO₂ coverage on Pd (111) and its effect on CH₄ dissociation

Experimental results demonstrate that complete CH_4 oxidation is the major reaction during O_2 removal. Therefore,

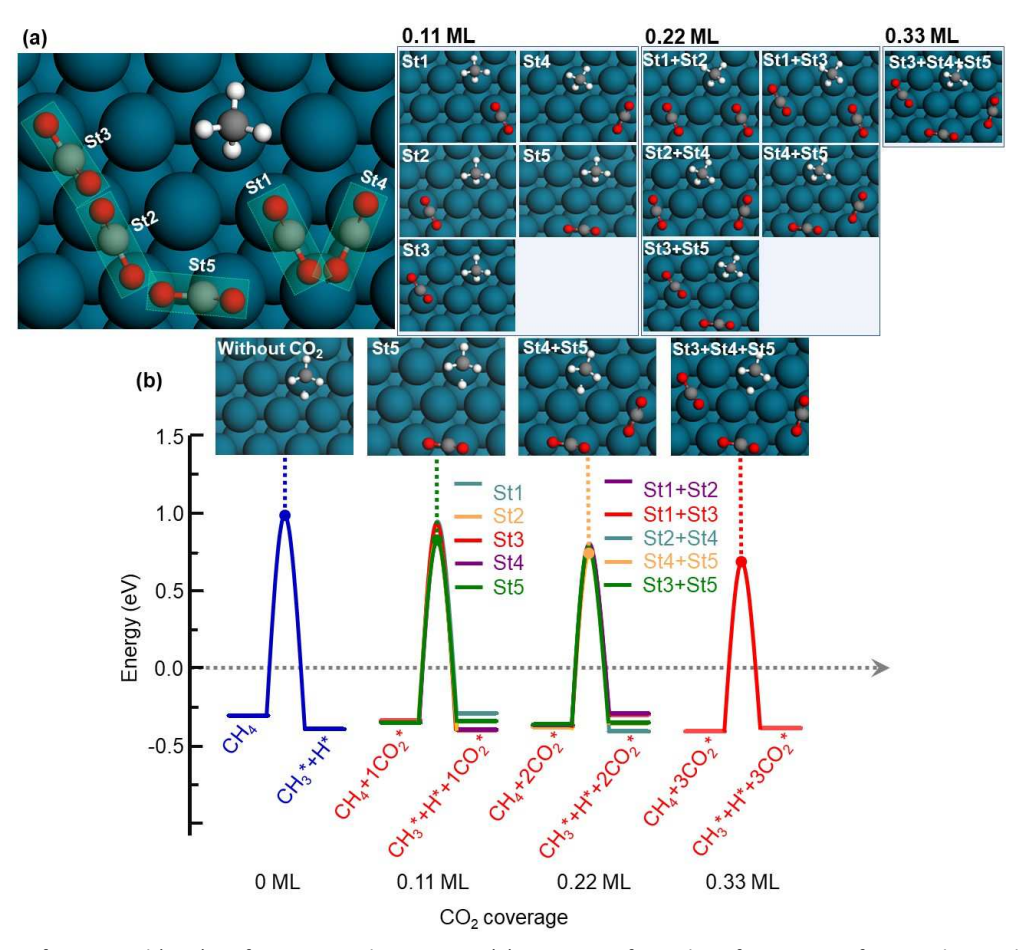


Fig 3. Coverage effect of CO_2 on Pd (111) surface on CH_4 dissociation. (a) Top view of initial configurations of CH_4 and CO_2 adsorbed on Pd (111) surface with various surface CO_2 coverages. (b) Energy diagrams of CH_4 dissociation with different surface CO_2 coverages and configurations. Inset shows top view of intermediates and adsorbed CO_2 on Pd (111) of specific surface CO_2 coverage showing the minimum activation energy. Blue, red, grey, and white atoms represent Pd, O, C, and H atoms, respectively.

Table 1. Reaction energies and activation energies for CH₄ dissociation with various surface CO₂ coverages.

Surface CO ₂ coverage				Surface HOCO coverage			
Coverage (ML)	Configuration	E_a (eV)	ΔE (eV)	Coverage (ML)	Configuration	E_a (eV)	ΔE (eV)
0	-	1.29	-0.090	0	-	1.29	-0.090
0.11	St1	1.28	0.050				
	St2	1.18	-0.055	0.11	St1	1.28	-0.067
	St3	1.29	-0.064		St2	1.22	0.083
	St4	1.17	-0.046		St3	1.24	-0.048
	St5	1.16	0.010				
0.22	St1+St4	1.18	-0.033				
	St1+St5	1.12	0.026	0.22	St2+St3	1.12	0.181
	St2+St3	1.17	0.062		St1+St3	1.18	-0.039
	St2+St4	1.17	0.074		St1+St2	1.28	0.102
	St3+St5	1.15	0.013				
0.33	St1+St3+St5	1.10	0.021	0.33	St1+St2+St3	1.25	0.304
Average	0	1.28	-0.090	Average	0	1.28	-0.090
	0.11	1.22	-0.021		0.11	1.25	-0.010
	0.22	1.16	0.029		0.22	1.19	0.081
	0.33	1.10	0.013		0.33	1.25	0.304

further calculations were performed based on completed CH₄ oxidation reactions. Previously, researchers have conducted extensive mechanistic studies of complete CH₄ oxidation with various catalysts.34-41 In those studies, reaction mechanisms and rate-limiting steps on the active catalytic surfaces under different conditions have been reported. Experimental studies revealed gaseous intermediates and products, such as CO and CO₂, by using gas chromatography, and also elucidated adsorbed surface intermediates, such as formate and carbonate species, by using in-situ diffuse reflectance infrared Fourier transform spectroscopy (in situ DRIFTS) analyses, which were used to conclude possible reaction pathways.34-36 Theoretical studies investigated various reaction pathways and their activation energy barriers to find the overall reaction pathways and the reaction energy landscape. 37-40 It is widely accepted that the dissociation of CH₄ is the rate-limiting step.^{38, 40} As a first step, various CO₂ coverages (0.11 ML, 0.22 ML, and 0.33 ML, ML is monolayer) on Pd (111) surface were used to investigate their effect on the CH₄ dissociation. Since the adsorption energy of CO₂ is very weak (~ 0.03 eV), and it has been proved that chemisorbed CO₂ can easily diffuse on Pd(111) surface by crossing a low barrier,28 we assume that CO2 can adsorb on different sites of Pd (111) surface (Fig 3a). Depending on relative positions between CO₂ and CH₄, we consider their different combination on Pd (111) surface for 0.22 ML and 0.33 ML, and these structures are chosen because they are most compacted on Pd (111) surface, and their surface coverage match well with experimental observations. Reaction energy $(\Delta E \ (eV) = E_{Final \ state} - E_{Initial \ state})$ and activation energy $(E_a, obtained from the saddle point energy)$ with and without CO2 were calculated and the results are shown in Fig 3b and Table 1. We can summarize four points here: Firstly, CH₄ dissociation without CO2 is a slightly exothermic reaction with an activation energy barrier of 1.29 eV. Secondly, regardless of different CO₂ coverage, the adsorption of CO₂ slightly reduced the energy of the initial structure (CH₄+xCO₂*, x=1 or 2 or 3, * indicates the adsorbed species), which indicates the enhanced adsorption of CH₄ on Pd (111) surface in the presence of CO₂. For example, the energy of the initial CH₄ with a CO₂ coverage of 0.33 ML shown in Fig 3a on Pd (111) surface is ~0.1 eV lower than that without CO2. Thirdly, the activation energy of CH4 dissociation with CO2 was lower than that without CO2, so, CO2 adsorption facilitates CH₄ reaction (Fig 4a). Fourthly, the activation energy of CH₄ dissociation was dependent on the CO₂ coverage. To clearly see the trend of CO₂ coverage and CH₄ dissociation, the activation energy of CH₄ dissociation is plotted as a function of CO₂ coverage on Pd (111) surface and is shown in Fig 4b. It can be observed that, as CO₂ coverage increases, the activation energy of CH₄ dissociation decreases, which implies that adsorbed CO₂ on Pd (111) promotes CH₄ dissociation and

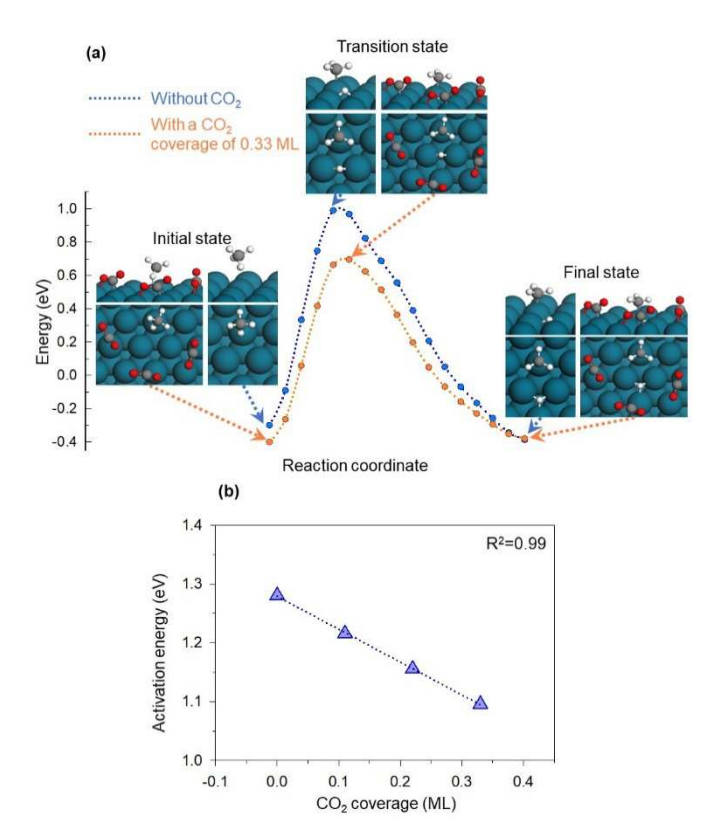


Fig 4. (a) Energy diagram of CH_4 dissociation without and with a CO_2 coverage of 0.33 ML, and (b) the variation of theoretically calculated activation energy with surface CO_2 coverage. Blue, red, grey, and white atoms represent Pd, O, C, and H atoms, respectively.

therefore, an increased CH_4 and O_2 conversion is expected. These results are consistent with our experimental observations (Figs 1d-f). We note that the ZPE corrections did not have any significant effect on the activation energy of CH_4 dissociation reaction under different surface CO_2 coverage (Table S2).

Reactions of CO₂ on Pd (111)

The effect of adsorbed CO₂ molecules and their coverage on CH₄ dissociation was revealed in previous section, and to fully understand our experimental detections, in this section, the possibility of other CO2 reactions on Pd (111) are further investigated. The schematic diagrams of potential reactions are shown in Fig 5a: (1) direct dissociation of CO_2 ($CO_2^* \rightarrow CO + O$); (2) reaction between CH₄ and chemisorbed CO₂ (CO₂* + CH₄ → HOCO* + CH₃*); (3) reaction with adsorbed CH₃ and chemisorbed $CO_2(CO_2^* + CH_3^* \rightarrow COOCH_3^*)$; (4) reaction with adsorbed H and chemisorbed CO_2 ($CO_2^* + H^* \rightarrow HOCO^*$) (* indicates the adsorbed species). Reactions 3 and 4 are related to the products of CH₄ dissociation, i.e., CH₃ and H. Four different adsorption sites (Fig S1⁺) were considered to determine the optimized initial and final structures, and their transition states. The results are shown in Fig 5b. Most of these side reactions have high activation energies. Specifically, the reaction with CH₄ has the highest activation energy (~ 2.65 eV), followed by the direct dissociation of CO₂ (~ 2.34 eV), adsorbed CH₃ (~ 2.10 eV), and the reaction with adsorbed H (~ 0.97 eV). Due to their high activation energies, we propose that, apart from the reaction between adsorbed H and chemisorbed CO₂, other reactions can hardly exist in our experiments. The activation energy of the reaction with adsorbed H is comparative with the reaction

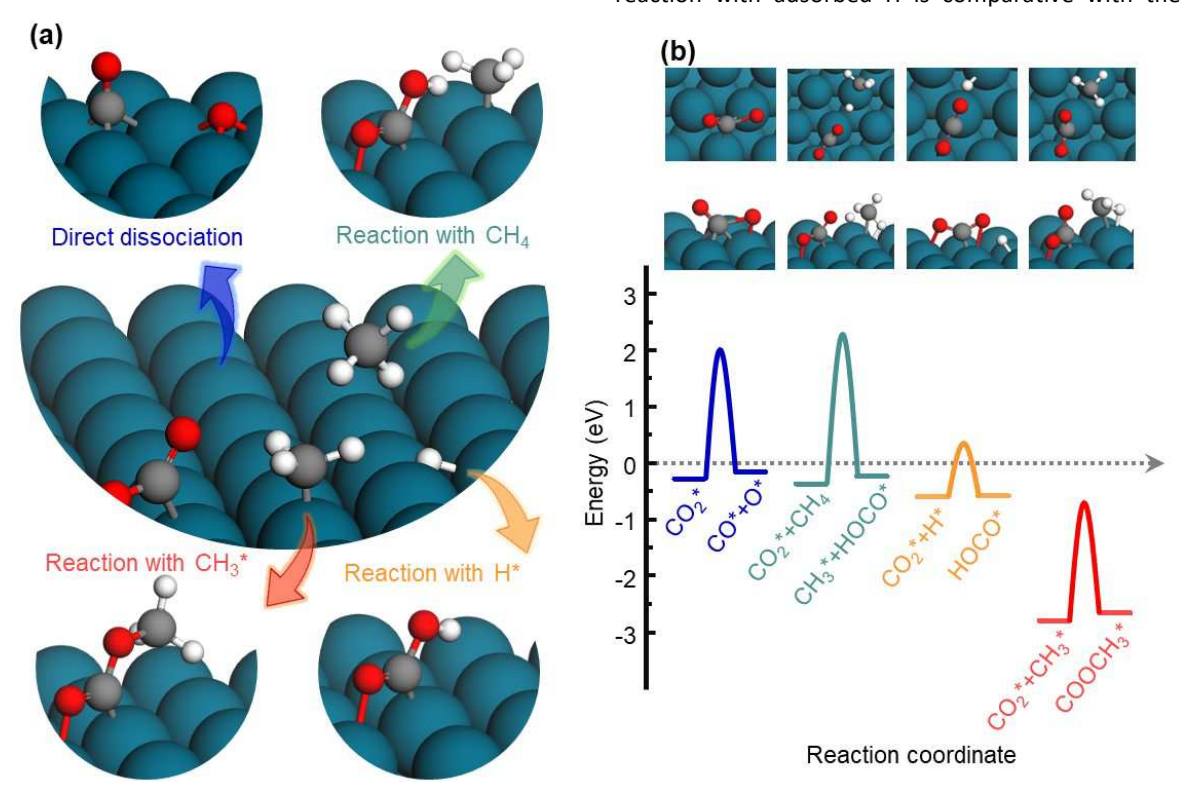


Fig 5. (a) Possible intermediates of various CO₂-involved side reactions on Pd (111) surface. (b) Energy diagram for various CO₂-involved reactions on the Pd (111) surface. The models at the top of the plot show the top view (top) and side view (bottom) of intermediates at the transition state. Blue, red, grey, and white atoms represent Pd, O, C, and H atoms, respectively.

between adsorbed O and adsorbed H ($^{\sim}$ 1.24 eV) (Fig S3†), which implies that adsorbed H possibly reacts with both adsorbed O and adsorbed CO₂. Therefore, the product (HOCO) from the reaction between adsorbed CO₂ and adsorbed H might affect the CH₄ dissociation as well.

HOCO coverage on Pd (111) and its effect on CH₄ dissociation

We further analyzed the effect of HOCO* coverage (0.11 ML, 0.22 ML, and 0.33 ML, ML is monolayer) — that can be produced during CO₂*+H*→HOCO* reaction — on CH₄ dissociation. Similar to the above studied CO₂ coverage effects, different adsorption sites were considered (inset in Fig 6a), and different HOCO and CH₄ combinations for 0.22 ML and 0.33 ML were considered. ΔE and E_a for CH₄ dissociation on Pd (111) with and without HOCO were calculated and the results are shown in Figs 6b and Table 1. According to the obtained results, we can conclude that, being similar to CO₂, HOCO also slightly promotes CH₄ adsorption on Pd (111) surface. It can be observed that the energy of the initial CH₄ with the HOCO coverage of 0.33 ML was ~0.05 eV lower than that without HOCO. The CH₄ dissociation with different HOCO coverages was mostly endothermic, i.e., higher energy at the final state compared to the initial state, and the activation energy of CH₄ dissociation was not strongly dependent on the adsorption site of HOCO on Pd (111). Moreover, the activation energies of CH₄ dissociation with HOCO coverages of 0.11 ML and 0.22 ML were

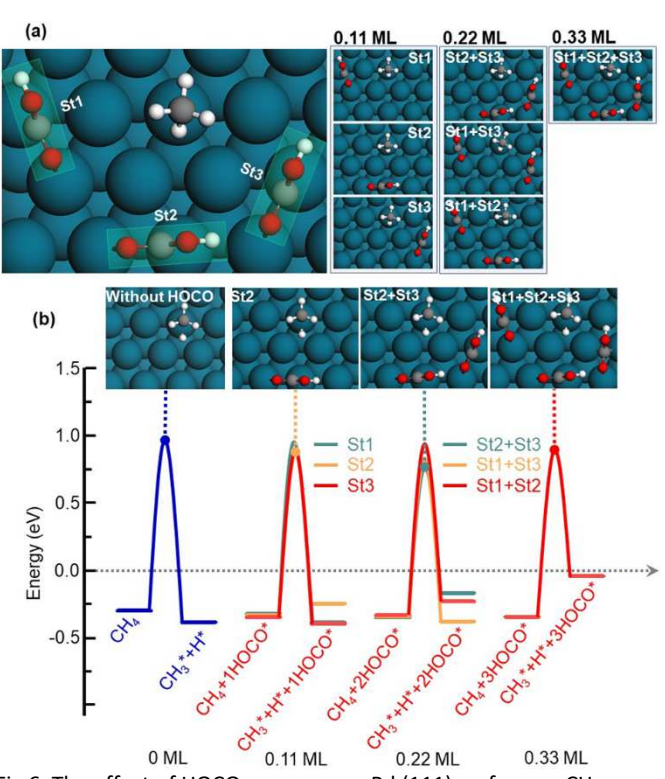


Fig 6. The effect of HOCO coverage on Pd (111) surface on CH_4 dissociation. (a) Top-view of initial configurations of CH_4 and HOCO adsorbed on a Pd (111) surface with various surface HOCO coverages. (b) Energy diagrams of CH_4 dissociation with different surface HOCO coverages. Inset shows top view of intermediates and adsorbed HOCO on Pd (111) of specific surface HOCO coverage showing the minimum activation energy. Blue, red, grey, and white atoms represent Pd, O, C, and H atoms, respectively.

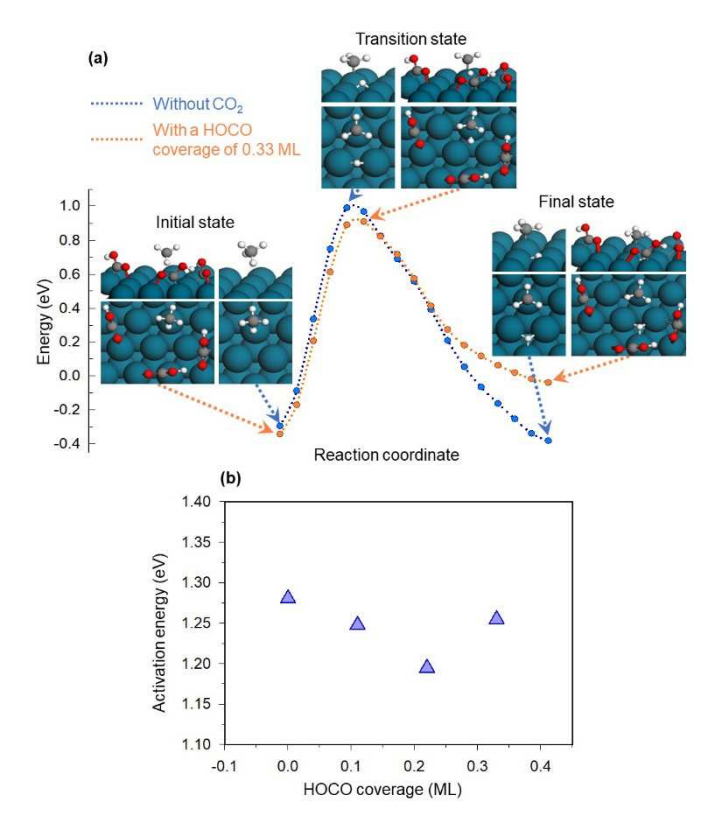


Fig 7. (a) Energy diagram of CH_4 dissociation without and with a HOCO coverage of 0.33 ML, and (b) the change in activation energy with increasing surface coverage of HOCO. Blue, red, grey, and white atoms represent Pd, O, C, and H atoms, respectively.

lower than that without HOCO, while under HOCO coverage of 0.33 ML, the activation energy was back to similar. These finding are clearly shown in energy diagram of CH₄ dissociation without HOCO and with a HOCO coverage of 0.33 ML in Fig 7a. To see the relation between HOCO coverage and CH₄ dissociation, the activation energy of CH₄ dissociation was plotted as a function of HOCO coverage (Fig 7b). It shows that the activation energy of CH₄ dissociation decreased with lower HOCO coverage on Pd (111) (0.11 ML and 0.22 ML). However, it increased with the highest HOCO coverage (0.33 ML), which indicates that high HOCO coverage is not favorable for CH₄ dissociation. Based on all these results, it can be concluded that CH₄ dissociation with HOCO coverage on Pd (111) surface is endothermic and has a higher activation than dissociation in the presence of CO2; therefore, the HOCO catalytic effects on CH₄ adsorption and reaction are less efficient than that of CO₂. Similar to the case of CH₄ dissociation under different surface CO₂ coverage, the ZPE corrections did not have any significant effects on the activation energy of CH₄ dissociation under different surface HOCO coverage (Table S2).

Potential energy profile with CO₂ coverage

Based on above findings, CO_2 coverage was found to accelerate CH_4 oxidation by reducing energy barriers of decomposition from CH_4 to CH_3^* and H^* . In this section, the effect of CO_2 coverage (0.33 ML) on overall complete CH_4 oxidation was investigated and the energy profile of complete CH_4 oxidation with CO_2 coverage is presented in Fig 8 and Table

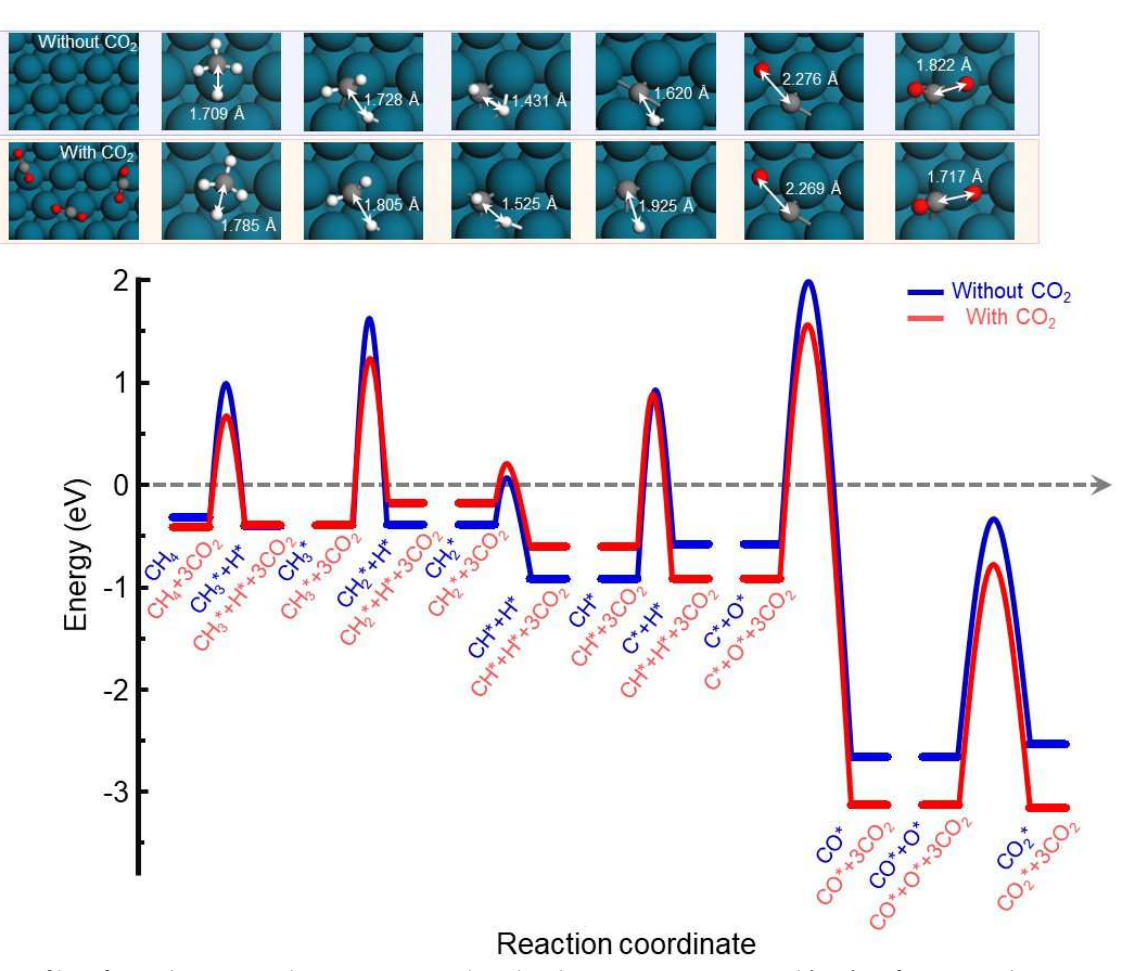


Fig 8. Energy profiles of complete CH_4 oxidation reaction with and without CO_2 coverage on Pd (111) surface. Inset shows top view of intermediates on Pd (111) surface. Blue, red, grey, and white atoms represent Pd, O, C, and H atoms, respectively.

S3. It can be found that complete CH₄ oxidation reaction was also sensitive to surface CO₂ coverage and that the activation energy is reduced by the increased surface coverage of CO₂. For example, lower activation energy barriers were distinct in the dissociation process of CH3 into CH2 and H (1.73 eV without surface CO₂ coverage vs. 1.64 eV with surface CO₂ coverage), and that in the dissociation of CH into C and H (1.86 eV without surface CO₂ coverage vs. 1.48 eV with surface CO₂ coverage). Transition states of all reactions without surface CO₂ coverage are presented in the blue region in the inset in Fig 8, and those with surface CO₂ coverage are depicted in the red region inset of Fig 8. As can be seen in Fig 8, the distances between C and dissociated H were extended with surface CO₂ coverage during CH_4 dissociation ($CH_4^* \rightarrow CH_3^* + H^*$), CH_3 dissociation ($CH_3^* \rightarrow$ $CH_2^*+H^*$), CH_2 dissociation ($CH_2^* \rightarrow CH^*+H^*$), and CH dissociation $(CH^* \rightarrow C^*+H^*)$. For example, the distance between C and dissociated H from CH₃ was 1.805 Å with surface CO₂ coverage, which is longer than 1.728 Å without surface CO₂ coverage. On the other hand, the distances between C and reacted O were shortened under surface CO₂ coverage during CO formation $(C^*+O^*\rightarrow CO^*)$ and CO_2 formation $(CO^*+O^*\rightarrow CO_2^*)$. For instance, the distance between C and reacted O in the reaction of CO2 formation was 1.717 Å with surface CO₂ coverage, while it was 1.822 Å without surface CO₂ coverage. This modified structure might be attributed to the variation of charge density distribution under different surface CO₂ coverage and is consistent with result of Wu *et al.*,¹⁸ which reports a charge transfer due to the modification of the charge density with surface HOCO coverage.

Conclusions

The effect of the excessive amount of CO₂ in the feed stream on O2 removal with CH4 oxidation was investigated by combining experimental and theoretical approaches. All reactions on the surface of Pd-TiO₂ catalyst synthesized via an aerosol route, are experimentally studied. Experimental results revealed that there was only one major CH₄ oxidation reaction, and the increase of the CO₂ concentration in the feed stream accelerates the generation rate of CO2. DFT calculations on Pd (111) surface show that the surface CO₂ coverage determines the rate-limiting step of the complete CH₄ oxidation reaction, and the increased surface CO₂ coverage reduces the barriers of CH₄ dissociation. The CO₂-containing intermediates (COOCH₃ and CO) are predicted to be not feasible because of their high activation energy barriers, and high coverage of HOCO inhibits the dissociation of CH₄ on Pd surface. Calculations of the energetics of the complete CH₄ reaction process show that CO₂ coverage accelerates complete CH₄ oxidation by lowering the activation energy barriers of several intermediates. All these findings emphasize the important role of CO₂ on the purification

process of remnant O_2 in the flue gas via complete CH_4 oxidation reaction from the oxy-combustion system. It provides a new positive aspect of the oxy-combustion system for purification of flue gas from the system due to the CO_2 -rich environment in it.

Conflicts of interest

There are no conflicts to declare.

Acknowledgements

This work was supported by a grant funded by the U.S. Department of Energy's National Energy Technology Laboratory under Award Number DE-FE0029161. R.M. acknowledges support from the National Science Foundation (NSF) through grants CBET-1729787, DMR-1931610 and DMR-1806147. This work used computational resources through allocation DMR160007 from the Extreme Science and Engineering Discovery Environment (XSEDE), which was supported by NSF ACI-1548562.

Supplementary material

Structure of Pd (111) and its adsorption sites, optimized structures of adsorbed molecules, activation energy by image optimization, NEB, and CI-NEB, reaction rates of CH_4 , $1/2O_2$, and 1/2CO with different conditions, OH formation on Pd (111), and reaction and activation energies for elementary reaction steps on Pd (111).

References

- B. J. P. Buhre, L. K. Elliott, C. D. Sheng, R. P. Gupta and T. F. Wall, *Prog Energ Combust*, 2005, **31**, 283-307.
- 2. A. Gopan, B. M. Kumfer, J. Phillips, D. Thimsen, R. Smith and R. L. Axelbaum, *Appl Energ*, 2014, **125**, 179-188.
- 3. K. Jordal, M. Anheden, J. Yan, L. Strömberg, *Greenhouse Gas Control Technologies*, 2005, **7**, 201-209.
- M. Kanniche, R. Gros-Bonnivard, P. Jaud, J. Valle-Marcos, J. M. Amann and C. Bouallou, Appl Therm Eng, 2010, 30, 53-62
- 5. Z. X. Dai, R. Middleton, H. Viswanathan, J. Fessenden-Rahn, J. Bauman, R. Pawar, S. Y. Lee and B. McPherson, *Environ Sci Tech Let*, 2014, **1**, 49-54.
- 6. W. N. Wang, W. J. An, B. Ramalingam, S. Mukherjee, D. M. Niedzwiedzki, S. Gangopadhyay and P. Biswas, *J Am Chem Soc*, 2012, **134**, 11276-11281.
- A. Dwivedi, R. Gudi and P. Biswas, J CO2 Util, 2018, 24, 376-385.
- 8. S. Chu, Science, 2009, **325**, 1599-1599.
- M. Woods and M. Matuszewski, Quality guidelines for energy system studies: CO2 impurity design parameters, NETL/DOE-341/011212; National Energy Technology Laboratory (NETL): Pittsburgh, PA, 2012.
- F. Ortloff, J. Bohnau, F. Graf and T. Kolb, Appl Catal B-Environ, 2016, 182, 375-384.
- Q. H. Zheng, S. J. Zhou, M. Lail and K. Amato, *Ind Eng Chem Res*, 2018, 57, 1954-1960.

- A. N. Kuhn, Z. Chen, Y. Lu and H. Yang, Energy Technol-Ger, 2019, 7, 1800917.
- A. N. Kuhn, Y. L. Ma, C. Zhang, Z. T. Chen, M. Y. Liu, Y. Q. Lu and H. Yang, *Energy Technol-Ger*, 2020, 8, 1901213.
- S. Jung, N. Reed, G. Yablonsky and P. Biswas, *Catal Sci Technol*, 2021, 11, 4763-4775.
- 15. A. J. Bissette and S. P. Fletcher, *Angew Chem Int Edit*, 2013, **52**, 12800-12826.
- Y. Yang, C. A. Mims, D. H. Mei, C. H. F. Peden and C. T. Campbell, J Catal, 2013, 298, 10-17.
- A. E. Masunov, E. Wait and S. S. Vasu, J Phys Chem A, 2016, 120, 6023-6028.
- 18. P. P. Wu and B. Yang, ACS Catal, 2017, **7**, 7187-7195.
- K. R. Hahn, M. Iannuzzi, A. P. Seitsonen and J. Hutter, *J Phys Chem C*, 2013, 117, 1701-1711.
- V. Tiwari, J. Jiang, V. Sethi and P. Biswas, Appl Catal A-General, 2008, 345, 241-246.
- G. Kresse and J. Furthmuller, *Phys Rev B*, 1996, **54**, 11169-11186.
- 22. P. E. Blöchl, Phys Rev B, 1994, **50**, 17953.
- J. P. Perdew, K. Burke and M. Ernzerhof, *Phys Rev Lett*, 1996, 77, 3865-3868.
- 24. H. J. Monkhorst and J. D. Pack, *Phys Rev B*, 1976, **13**, 5188.
- S. Grimme, S. Ehrlich and L. Goerigk, *J Comput Chem*, 2011,
 1456-1465.
- S. W. Yang, A. Maroto-Valiente, M. Benito-Gonzalez, I. Rodriguez-Ramos and A. Guerrero-Ruiz, Appl Catal B-Environ, 2000, 28, 223-233.
- K. Murata, D. Kosuge, J. Ohyama, Y. Mahara, Y. Yamamoto,
 S. Arai and A. Satsuma, *ACS Catal*, 2019, 10, 1381-1387.
- 28. L. S. Xuejing Liu, Wei-Qiao Deng, *J Phys Chem C*, 2018, **122**, 8306-8314.
- 29. H. Jónsson, G. Mills and K. W. Jacobsen, 1998, 385-404.
- R. Gholizadeh and Y.-X. Yu, Appl Surf Sci, 2015, 357, 1187-1195.
- 31. S. Pennycook and D. Jesson, *Ultramicroscopy*, 1991, **37**, 14-
- 32. F. Niu, S. Q. Li, Y. C. Zong and Q. Yao, *J Phys Chem C*, 2014, **118**, 19165-19171.
- 33. M. H. Zhang, Y. F. Wu, M. B. Dou and Y. Z. Yu, *Catal Lett*, 2018, **148**, 2935-2944.
- 34. O. Demoulin, M. Navez and P. Ruiz, *Appl Catal A-General*, 2005, **295**, 59-70.
- M. Schmal, M. M. V. M. Souza, V. V. Alegre, M. A. P. da Silva, D. V. Cesar and C. A. C. Perez, *Catal Today*, 2006, **118**, 392-401.
- 36. P. Gelin and M. Primet, Applied Catalysis B-Environmental, 2002, **39**, 1-37.
- A. Trinchero, A. Hellman and H. Gronbeck, Surf Sci, 2013, 616, 206-213.
- 38. A. D. Mayernick and M. J. Janik, *J Catal*, 2011, **278**, 16-25.
- J. S. Yoo, J. Schumann, F. Studt, F. Abild-Pedersen and J. K. Norskov, *J Phys Chem C*, 2018, **122**, 16023-16032.
- M. Jorgensen and H. Gronbeck, ACS Catal, 2016, 6, 6730-6738
- Y. H. (Cathy) Chin, C. Buda, M. Neurock and E. Iglesia, J Am Chem Soc, 2011, 133, 15958-15978.